JOURNAL OF MATERIALS SCIENCE 30 (1995) 5381–5388

The electrochemical properties of Li_3AlN_2 and Li_2SiN_2

M. S. BHAMRA
Department of Materials Science and Metallurgy, University of Cambridge, Cambridge CB2 3QZ, UK

D. J. FRAY
Department of Mining and Mineral Engineering, University of Leeds, Leeds LS2 9JT, UK

Lithium ion-conducting solid electrolytes Li_3AlN_2 and Li_2SiN_2 were investigated as possible electrolytes for nitrogen sensors. The nitride ceramics were synthesized and characterized by SEM, X-ray diffraction and a.c. impedance. Thermodynamic measurements were carried out by measuring cell electromotive forces (e.m.f.s) consisting of solid electrolyte tubes sandwiched between Cr/Cr_2N and CrN/Cr_2N references. The results corresponded to the values given in the literature for this system.

1. Introduction

There is a need to be able to analyse accurately and quickly elements in metallic solutions at elevated temperatures. This applies particularly when a refining process is taking place or when producing alloy castings where a minor constituent in the melt can have a major effect upon the properties of the finished product. Nitrogen, being the major constituent of air, can easily dissolve in molten steel and is present in all steels and affects the properties of the alloy [1]. Some effects are beneficial, others are detrimental. It can be present as free atomic nitrogen, unstable nitrides, firmly bonded nitrides and carbon nitrides, each effecting the metallurgical properties in a different way, but by controlling the heat treatment it is possible to control the phase that is present. The detrimental effects of nitrogen can be associated with embrittling phenomena and this can have severe consequences for continuous casting of sheet steel, welding and hot ductility. The beneficial effects of nitrogen in steel includes increased strength, toughness, corrosion resistance and improved creep and fatigue life.

Most of the methods used for detecting nitrogen require that a sample is taken and sent for analysis [2–4]. Chemical analysis, which takes several hours, has been used as well as methods which rely on the nitrogen being extracted and the gas analysed by gas chromatography or a catherometer. Recently a device has been developed in which argon bubbles equilibrate with nitrogen in the melts and the gas is then analysed.

An improved method of analysis would be a sensor, based upon a solid electrolyte [5]. If there is a concentration difference across a solid electrolyte a potential is generated which is related logarithmically to the concentration, i.e.

$$-ZEF = RT \ln \frac{a'_x}{a''_x} \quad (1)$$

where Z is the charge carried, E is the potential, F is Faraday's constant, R is the gas constant, T is the temperature and a' and a'' are the activities of x on either side of the electrolyte which is a conductor of x ions. In order to make such a sensor, it is necessary to fix the concentration of x on one side of the electrolyte: for a nitrogen sensor, Cr_2N/Cr or Ta_2N/Ta, etc., could be used. The selection of the electrolyte is much more difficult as there are no electrolytes where the mobile ion is nitrogen. One way of overcoming this problem is to use a lithium-conducting electrolyte which contains nitrogen, such as Li_3N, Li_3AlN_2 and $Li_xSi_yN_z$.

In these cases, the compound essentially dissociates at the surface to form nitrogen. In the case of Li_3N, the following occurs

$$Li_3N \rightleftharpoons 3Li + \frac{1}{2}N_2 \quad (2)$$

$$K = \frac{a_{Li}^3 P_{N_2}^{1/2}}{a m_{Li_3N}} \quad (3)$$

As the activity of a the solid electrolyte, Li_3N, is fixed, any change in the partial pressure P or activity of nitrogen results in a change in the activity of lithium on the surface of the electrolyte and this is detected by the solid electrolyte.

However, lithium nitride suffers from the disadvantages of self ignition when in contact with air (especially when it is finely divided), a low thermodynamic decomposition potential and a low melting point [6, 7]. It is, therefore, important to consider other nitrogen-containing solid electrolytes which are more stable.

Juza and Hund [8] originally prepared lithium aluminium (Li_3AlN_2), which can be represented by the general formula of $Li_{2x-3}M^{x+}N_{x-1}$. It crystallizes in a cubic cell with a lattice parameter of $a = 0.946$ nm and belongs to the space group T_7^h. Yamane *et al.* [9] measured the room temperature conductivity of

0022–2461

TABLE I Phases of lithium silicon nitride [14]

Phase		Crystal structure	Lattice parameter (nm)
I	$LiSi_2N_3$	Orthorhombic	–[a]
II	Li_2SiN_2	NA	–[a]
III	Li_5SiN_3	Cubic	$a = 0.472$
IV	$Li_{18}Si_3N_{10}$	Tetragonal	$a = 1.417$, $c = 1.435$
V	$Li_{21}Si_3N_{11}$	Tetragonal	$a = 0.942$, $c = 0.953$
VI	Li_8SiN_4	Tetragonal	$a = 1.022$, $c = 0.954$

[a] Not available.

TABLE II Ionic conductivity and activation energy of lithium silicon nitrides [14]

	σ_{400K} ($\Omega^{-1}\,cm^{-1}$)	E_a (eV)
$LiSi_2N_3$	1.9×10^{-7}	0.66
Li_2SiN_2	1.1×10^{-5}	0.55
Li_5SiN_3	4.7×10^{-5}	0.59
$Li_{18}SiN_{10}$	2.9×10^{-5}	0.57
$Li_{21}Si_3N_{11}$	8.6×10^{-6}	0.56
Li_8SiN_4	5.0×10^{-4}	0.47

Li_3AlN_2 to be $5 \times 10^{-8}\ \Omega^{-1}\,cm^{-1}$ with an activation energy of 0.54 eV. The electronic conductivity was found to be negligible.

Several phases of lithium silicon nitride ternary compounds ($Li_xSi_yN_2$) have been reported by several different authors. Juza *et al.* [10] prepared Li_5SiN_3 which has an antifluorite superstructure, and Lang and Charlot [11] synthesized of $LiSi_2N_3$, Li_2SiN_2 and Li_8SiN_4. Dadd and Hubberstey [12] synthesized Li_5SiN_3 which crystallized in the cubic system, and David *et al.* [13] determined the crystal structure of $LiSi_2N_3$ as wurtzite. The crystal structure of Li_2SiN_2 has not been determined. Table I describes all the phases of lithium silicon nitrides with lattice parameters and crystal type. All six phases of lithium silicon nitride have been identified by Yamane *et al.* [14] as (i) $LiSi_2N_3$, (ii) Li_2SiN_2, (iii) Li_5SiN_3, (iv) $Li_{18}Si_3N_{10}$, (v) $Li_{21}Si_3N_{11}$ and (vi) Li_8SiN_4. The phase Li_8SiN_4 was found to have the highest ionic conductivity as shown in Table II, but was found to be the most unstable in air. The electronic conductivity was found to be negligible in all the phases.

As a possible reference system it was decided to investigate chromium and molybdenum and their nitrides.

Chromium forms two nitrides, Cr_2N and CrN, and these have broad regions of homogeneity. Mills [15, 16] calculated the equilibrium pressure for the decomposition of the two nitrides as shown in Equations 4 and 5

$$2Cr + \frac{1}{2}N_2 \rightarrow Cr_2N \quad (4)$$

$$Cr_2N + \frac{1}{2}N_2 \rightarrow 2CrN \quad (5)$$

For the Cr-Cr_2N equilibrium as shown in Equation 4 the data plotted appeared in a straight line expressed by

$$\log P_1 = -\frac{11\,680}{T} + 5.79 \quad (6)$$

For the Cr_2N–CrN equilibrium in Equation 5, the data plotted appeared in a straight line expressed by

$$\log P_2 = -\frac{10\,620}{T} + 8.03 \quad (7)$$

where P is the equilibrium pressure (atm), and T is the temperature (K).

There are very few references to work done on the thermodynamics of dissociation of molybdenum nitride, but Wicks and Block [17] derived free-energy change functions for the equation of formation of dimolybdenum nitride as a function of temperature

$$2Mo + \frac{1}{2}N_2 = Mo_2N \quad (8)$$

$$\Delta G^{\ominus} = (-16\,150 + 3.10T\ln T - 5.34 \times 10^{-3}T^{-2} - 1.98T)\,J \quad (9)$$

2. Experimental procedure

2.1. Synthesis and fabrication of solid electrolytes and metal/metal nitride mixtures

2.1.1. Li_3AlN_2

The starting materials used for synthesizing Li_3AlN_2 were lithium nitride (Johnson Matthey Alpha Products) and aluminium nitride (Aldrich Chemical Co.). The powders were weighed out in a 1.25:1 ratio of Li_3N:AlN with Li_3N in excess, because it was shown by Yamane *et al.* [9] that this stops contamination from AlN. The powders were mixed and then calcined at 900 °C under ultra pure flowing nitrogen for 1 h and were milled in acetone using 5.9 mm diameter YSZ (yytria-stabilized zirconia) balls. Cylindrical pellets and tubes with one end open were formed by iso-pressing at 607 MPa and sintering at 1000 °C for 30 min under pure flowing nitrogen.

2.1.2. Li_2SiN_2

The starting materials used for synthesizing Li_2SiN_2 were Li_3N and α-phase Si_3N_4 (Aldrich Chemical Co.). The powders were weighed out in a 2:1 stoichiometric ratio of Li_3N: Si_3N_4, mixed and calcined at 802 °C for 30 min under ultra pure flowing nitrogen. The reaction product was milled in acetone and pellets and tubes were iso-pressed at 971 MPa. The compacts were sintered at 808 °C for 30 min under pure nitrogen.

All manipulations of the starting materials and reaction products of the above two solid electrolytes were carried out in a nitrogen-filled glove box. The density of all the samples were measured by an Archimedes'-based method using toluene as the liquid.

2.1.3. Nitrogen reference

(i) Chromium and dichromium nitride (Cr/Cr_2N) (Johnson Matthey) were mixed in a 1:1 ratio and iso-pressed into pellets at 935 MPa.

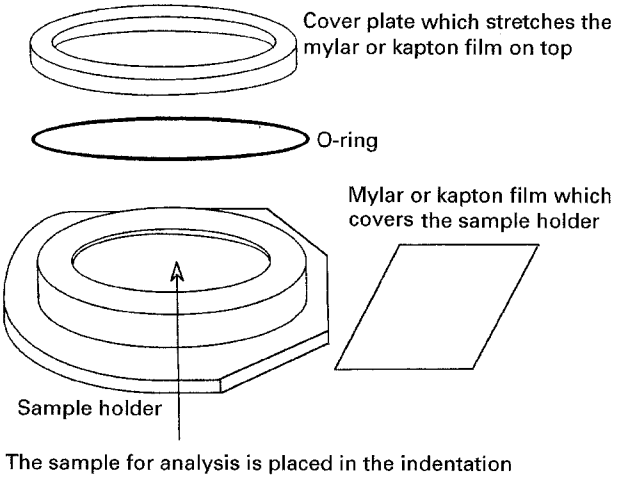

Figure 1 X-ray sample holder for moisture-sensitive materials.

(ii) Chromium nitride and dichromium nitride (CrN/Cr_2N) were mixed in a 1:1 ratio and used exclusively as a powder.

(iii) Molybdenum (Johnson Matthey) and dimolybdenum nitride (Koch Chemicals) ($MOMO_2N$) were mixed in a 1:1 ratio and iso-pressed at 935 MPa.

2.2. X-ray diffraction

Step-scanning diffractometry was carried out using a Philips vertical diffractometer with CuK_α radiation of 0.15417 nm. The diffractometer was calibrated using mica (muscovite) film and the samples had silicon as an internal reference during irradiation. As the nitride powders are moisture sensitive, a sample holder was designed, as shown in Fig. 1, which incorporated a mylar film to keep out air and moisture during irradiation.

2.3. Scanning electron microscopy

A Camscan (S2) scanning electron microscope using the secondary emission electron detector was used to examine microstructure and surfaces of the sinters. The samples were stuck on to aluminium stubs using silver paint and then sputtered with gold to improve electrical conduction.

2.4. Impedance spectroscopy

Electrochemical impedance measurements were carried out using a Solarton high-frequency response analyser, with an EG and G potentiostat galvanostat. Sintered pellets were polished with SiC paper and washed ultrasonically in acetone. The samples were sputtered with 1 μm silver or platinum on the flat surface to act as a blocking electrode.

2.5. Thermodynamic measurements

Li_2SiN_2 and Li_3AlN_2 tubes were placed between the solid-state nitrogen references and set up as a galvanic cell as shown in Fig. 2. Molybdenum or platinum electrodes were placed on the outside of the references and then connected to a high-impedance voltmeter.

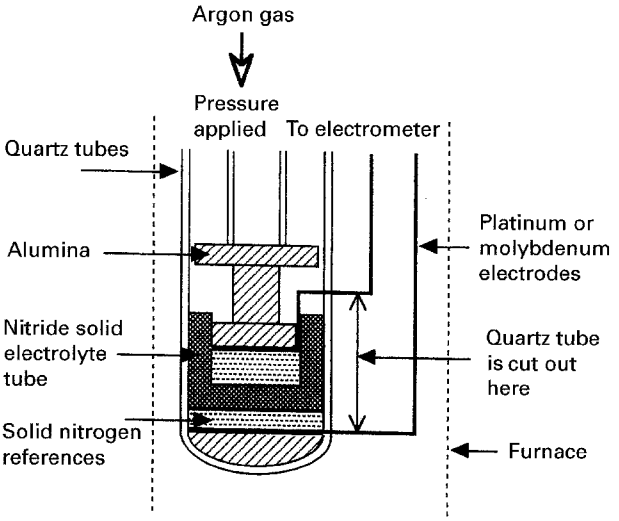

Figure 2 Cell used for thermodynamic measurements.

TABLE III Average particle size for calcined and milled powders

	Average particle size (μm)	
	Calcined	Milled
$Li_3Al_2N_2$	6.34	0.84
Li_2SiN_2	2.37	0.97

The furnace tube was earthed with a stainless steel cage and purged with high-purity 99.99% argon. The temperature of the cell was determined by a chromel–alumel thermocouple.

3. Results and discussion

3.1. Calcining and sintering Li_3AlN_2 and Li_2SiN_2

Three methods for sintering and calcining nitride ceramics were investigated: (i) firing in an alumina tube with free flowing nitrogen; (ii) firing in an enclosed quartz silica tube; and (iii) firing in an evacuated alumina tube. It was found that method (i) produced contaminated powders and sinters with surface oxidation, whereas methods (ii) and (iii) produced samples virtually free of contaminants. Method (iii) was found to be the best method as a wide range of sizes and shapes of samples could be fired and this method was adopted as the method for firing all the nitride ceramics.

3.2. Particle-size analysis

The average particle sizes of the calcined and milled powders are shown in Table III for milling with 5.9 mm diameter spheres of yttria-stabilized zirconia in acetone. The table shows that there was a satisfactory reduction in the size of the particles.

3.3. Density of sintered samples

3.3.1. Li_3AlN_2

The maximum green body density which could be achieved was 72%, at a pressure of 607 MPa. On

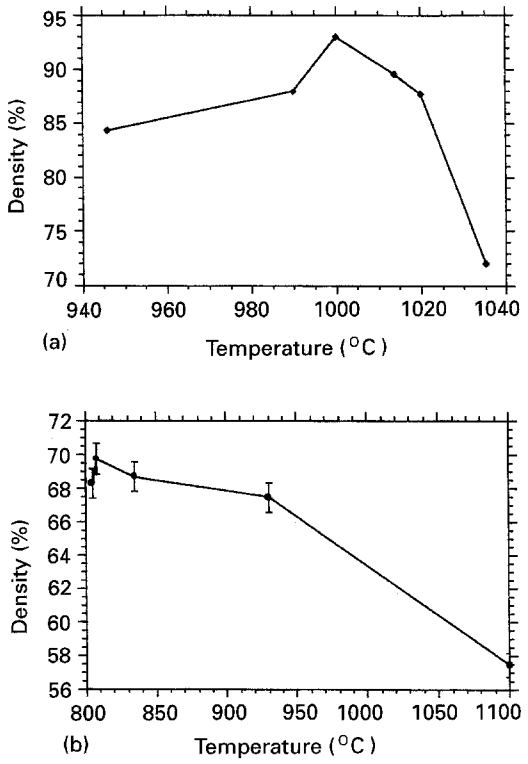

Figure 3 Density of (a) Li_3AlN_2 and (b) Li_2SiN_2 sinters as a function of temperature.

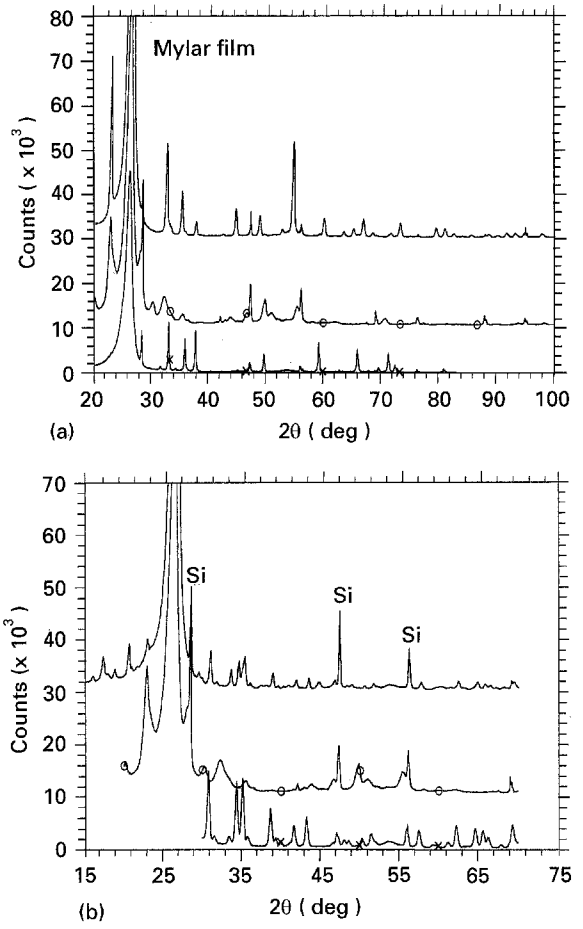

Figure 4 Solid-state synthesis of (a) Li_3AlN_2 and (b) Li_2SiN_2. (a) (—) Li_3AlN_2 reaction product, (O) Li_3N starting material, (x) AlN starting material; (b) (—) Li_2SiN_2 reaction product, (O) Li_3N starting material, (x) Si_3N_4 starting material, Si = silicon reference.

sintering, the maximum density of 93% was attained at 1000 °C. At temperatures greater than 1000 °C, the density dropped considerably due to the decomposition of the sample into AlN and Li_3N [8]. The density as a function of temperature is shown in Fig. 3a.

3.3.2. Li_2SiN_2

Pellets of this material, isopressed at 971 MPa and fixed at 808 °C gave a maximum density of 71% ± 2.6%, which decreased at higher and lower temperatures. An inspection of the sintered samples revealed a white porous surface layer which was easily removed to reveal a grey sinter but this only increases the density of 72% ± 2.6%. Sintering at higher temperatures resulted in the X-ray diffractogram showing an intense doublet as the peaks at 18.9° and 19.4° which could be attributed to $Li_{18}Si_3N_{10}$ and $LiSi_2N_3$, respectively. The density as a function of sintering temperature is shown in Fig. 3b.

3.4. X-ray diffraction

Li_3AlN_2 and Li_2SiN_2 were obtained as a single phase as shown in the X-ray diffractograms of Fig. 4a and b. The X-ray diffraction peaks of Li_3AlN_2 matched those of Juza and Hund [8] and the peaks of Li_2SiN_2 matched those of Yamane *et al.* [14].

3.5. A.c. conductivity

Impedance measurements were carried out on the most densely sintered pellets under ultra-clean nitrogen with platinum or silver blocking electrodes. The results were plotted as Nyquist plot with real Z' as the x-axis and the imaginary $-Z''$ as the y-axis.

3.5.1. Li_3AlN_2

3.5.1.1. Nyquist plots. Two sets of impedance plots are shown for samples with 90% densities in Fig. 5a–c with platinum electrodes and Fig. 5d–f with silver electrodes. Measurements were made over the temperature range 150–600 °C.

The complex impedance plots at 150° and 200 °C in Fig. 5a and d with platinum and silver electrodes, respectively, show a depressed semicircle going to the origin and a straight-line portion. The low-frequency portion extending back to the real axis was taken as the total conductivity. At 200 °C, Fig. 5d, two semicircles are evident, one for transcrystalline (high-frequency portion) and the other for intercrystalline (low-frequency portion) conductivity. The plots at 324 and 300 °C are shown in Fig. 5b and e, respectively, and only show half a semicircle. This is caused by the decrease in the time constant at higher temperatures and because the frequency response analyser only had a maximum limit of 10^5, only half a semicircle is discerned. At 600 °C, Fig. 5c and f, only a low-frequency portion is seen, which is not linear and this

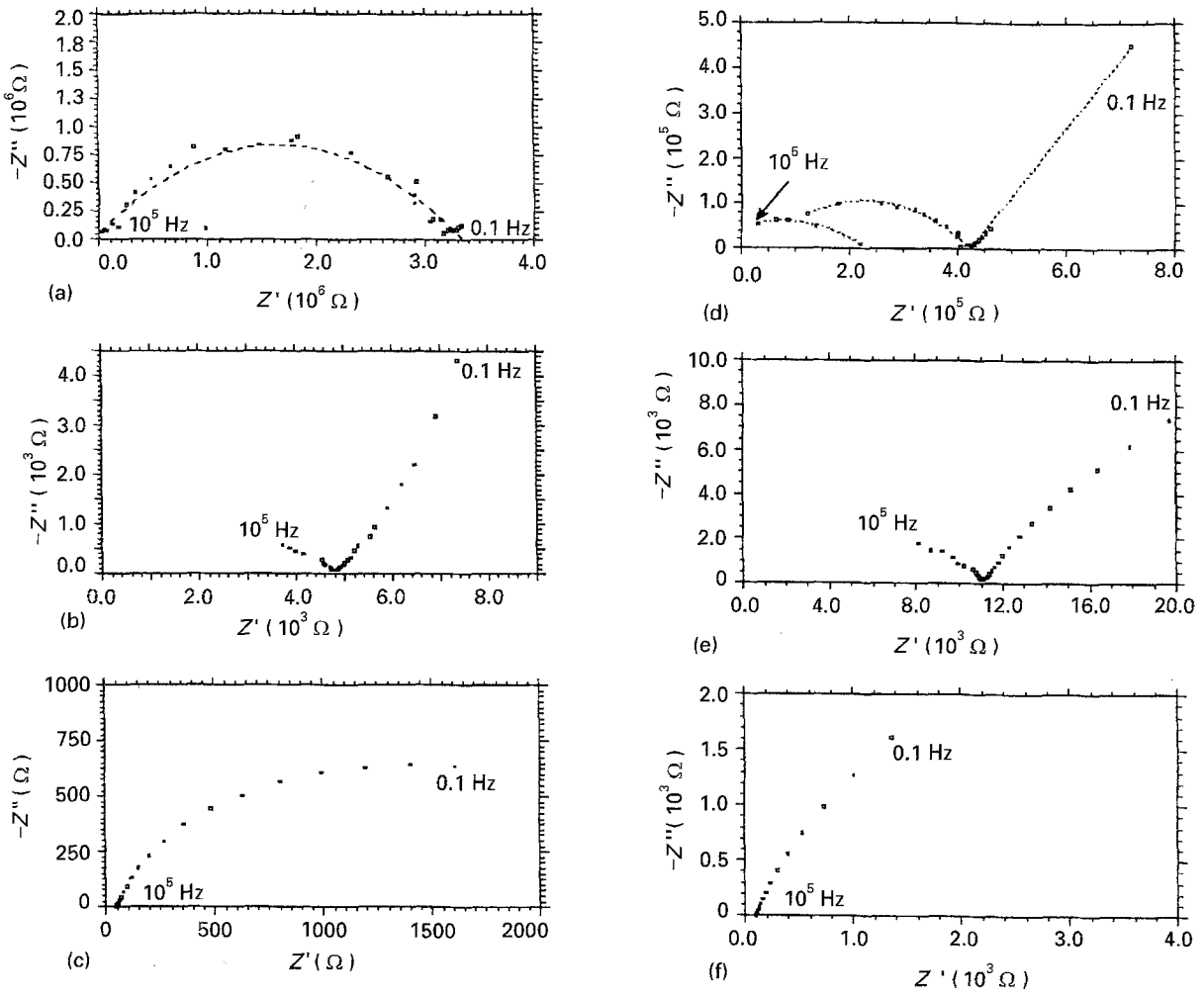

Figure 5 Complex plane impedance plots for Li_3AlN_2 with (a–c) platinum electrodes and (d–f) silver electrodes. (a) 150 °C, (b) 324 °C, (c) 600 °C, (d) 200 °C, (e) 300 °C, (f) 600 °C.

TABLE IV Experimental conductivity data for Li_3AlN_2 with platinum and silver electrodes

Platinum electrode, $E_{act} = 0.87 \pm 0.018$ eV		Silver electrode, $E_{act} = 0.85 \pm 0.033$ eV	
Temperature (°C)	Conductivity ($\Omega^{-1}\,cm^{-1}$)	Temperature (°C)	Conductivity ($\Omega^{-1}\,cm^{-1}$)
800	9.7×10^{-2}	800	0.1
700	3.3×10^{-2}	700	2.4×10^{-2}
600	7.6×10^{-3}	600	3.2×10^{-3}
500	1.8×10^{-3}	500	7.1×10^{-4}
400	3.7×10^{-4}	400	1.6×10^{-4}
324	6.8×10^{-5}	300	2.8×10^{-5}
150	1.0×10^{-7}	200	1.5×10^{-7}
		100	4.2×10^{-9}

non-linearity can be attributed to surface roughness and inhomogeneities of the bulk sample.

3.5.1.2. Conductivity. The conductivity data obtained from the impedance plots are shown in Table IV. Activation energy plots for both platinum and silver electrodes are shown in Fig. 6a and b. A straight line which followed the Arrhenius equation was observed which is similar to the work of Yamane *et al.* [9] who found similar impedance spectra with the following conductivity data, $\sigma = 5 \times 10^{-8}\,\Omega^{-1}\,cm^{-1}$ at 25 °C and an activation energy of 0.54 eV.

3.5.2. Li_2SiN_2

3.5.2.1. Nyquist plots. Fig. 7a–c and d–f show Li_2SiN_2 sinter sputtered with platinum and silver electrodes, respectively, over a range of temperatures from 135–600 °C. The density of Li_2SiN_2 was 69% ± 2.6% of the theoretical minimum. Complex impedance plots

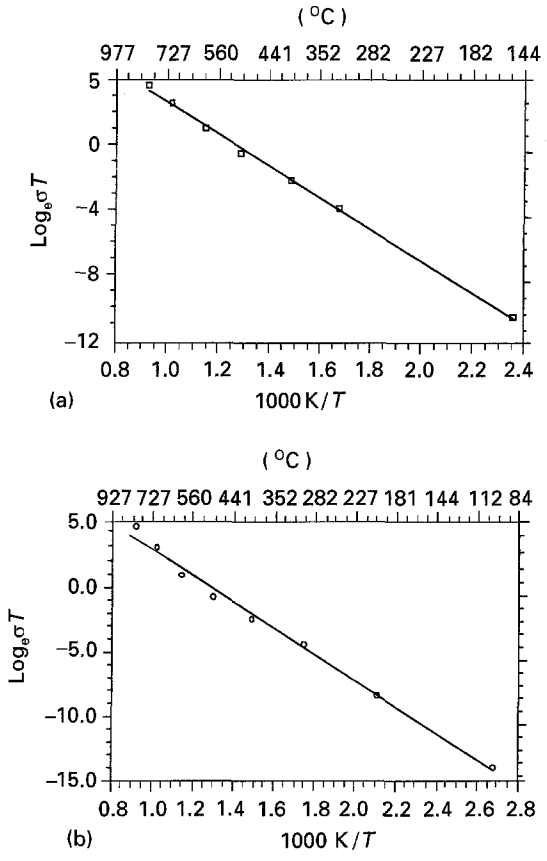

Figure 6 Conductivity plots for Li_3AlN_2 with (a) platinum and (b) silver electrodes.

with features similar to those of Li_3AlN_2 plots were obtained.

3.5.2.2. Conductivity. The conductivity data obtained from the impedance plots is shown in Table V. Activation energy plots for both platinum and silver electrodes are shown in Figs 8a and 9b. The activation energies were 0.68 ± 0.014 and 0.74 ± 0.02 eV for the platinum and silver electrodes, respectively. Yamane *et al.* [14] found values of $1.1 \times 10^{-8}\,\Omega^{-1}\,cm^{-1}$ at 127 °C and an activation energy of 0.55 eV.

3.6. Thermodynamic measurements

The experimental data with the Li_3AlN_2 solid electrolyte was found to be coherent and reproducible, whereas the data with Li_2SiN_2 was found to be inconsistent. Fig. 9 shows the dwell electromotive force (e.m.f.) for cell $Cr/Cr_2N|Li_3AlN_2|CrN/Cr_2N$ which follows the data of Mills [15, 16] closely at a temperature range of 750–850 °C. However, e.m.f. measurements taken above 850 °C were found to deviate markedly with those of Mills [15, 16]. It was revealed from the X-ray diffractogram of Fig. 10 that sintering Li_3AlN_2 at high temperatures (1035 °C) showed the presence of an extra phase which was identified as AlN as was also noted by Juza and Hund [8].

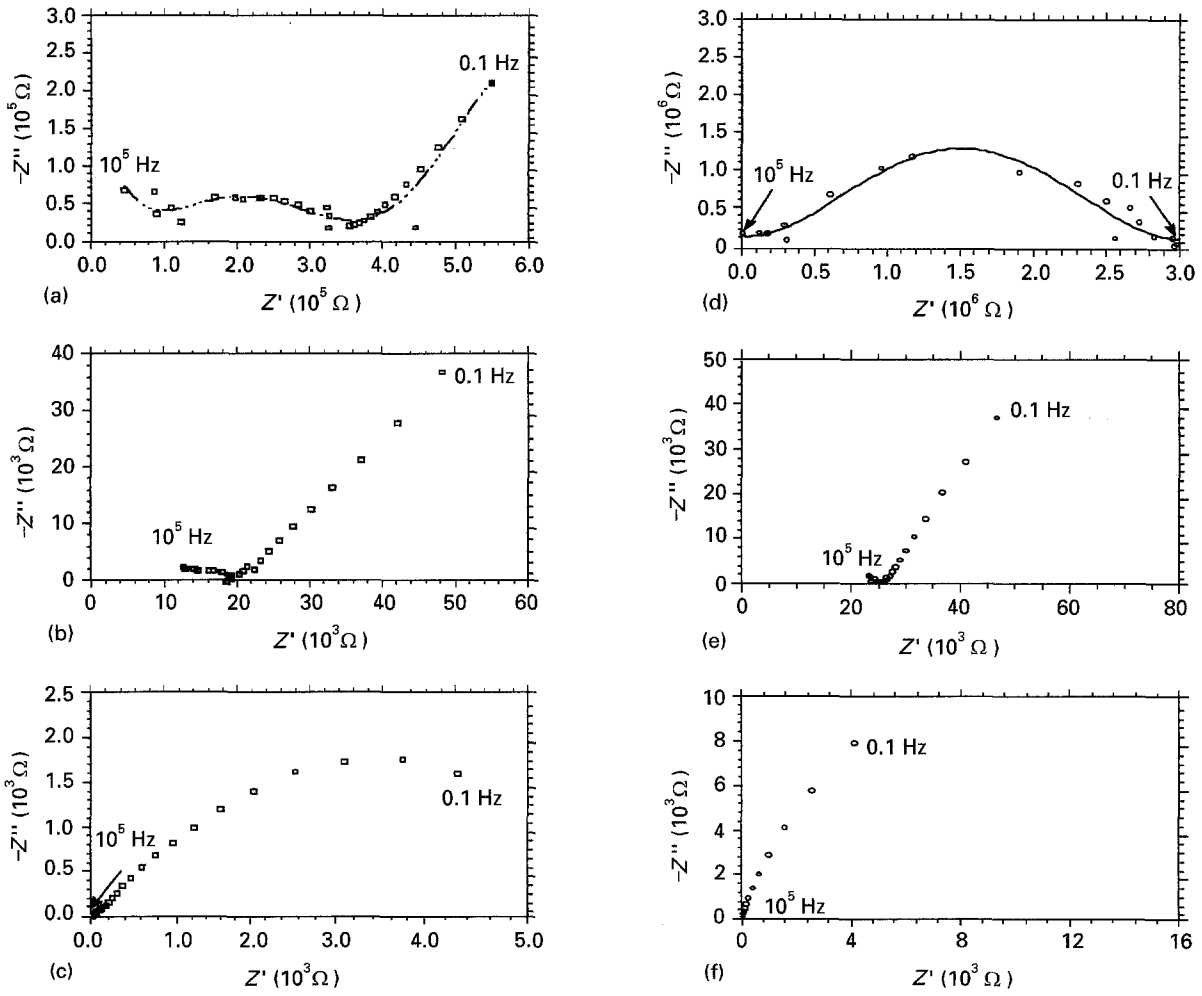

Figure 7 Complex plane impedance plots for Li_2SiN_2 with (a–c) platinum electrodes and (d–f) silver electrodes. (a) 135 °C, (b) 200 °C, (c) 600 °C, (d) 100 °C, (e) 200 °C, (f) 600 °C.

TABLE V Experimental conductivity data for Li_2SiN_2 with platinum and silver electrodes

Platinum electrode, $E_{act} = 0.68 \pm 0.014$ eV		Silver electrode, $E_{act} = 0.74 \pm 0.025$ eV	
Temperature (°C)	Conductivity ($\Omega^{-1}\,cm^{-1}$)	Temperature (°C)	Conductivity ($\Omega^{-1}\,cm^{-1}$)
800	5.4×10^{-2}	800	5.3×10^{-2}
700	4.0×10^{-2}	700	3.7×10^{-2}
600	9.0×10^{-3}	600	1.3×10^{-2}
500	4.0×10^{-3}	500	4.1×10^{-3}
400	1.1×10^{-3}	400	4.9×10^{-4}
333	2.6×10^{-4}	300	7.9×10^{-5}
200	1.3×10^{-5}	200	7.1×10^{-6}
131	6.9×10^{-7}		

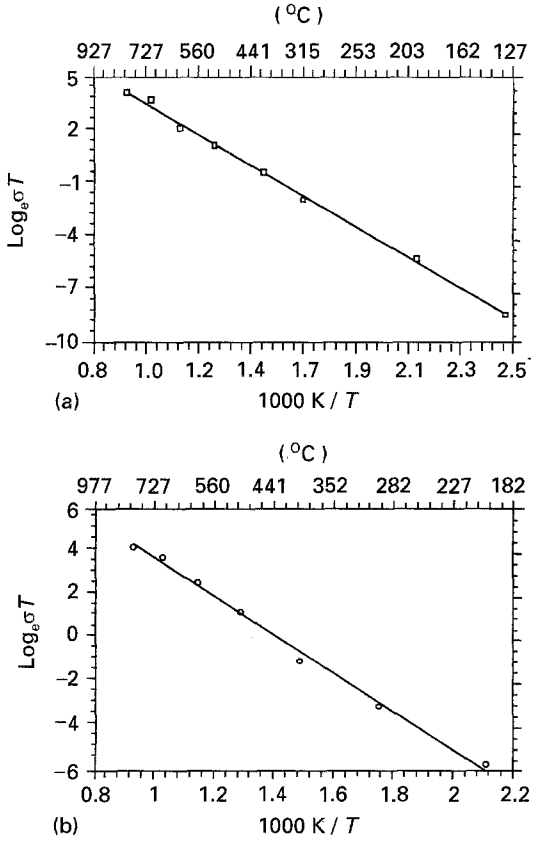

Figure 8 Conductivity plots for Li_2SiN_2 with (a) platinum and (b) silver electrodes.

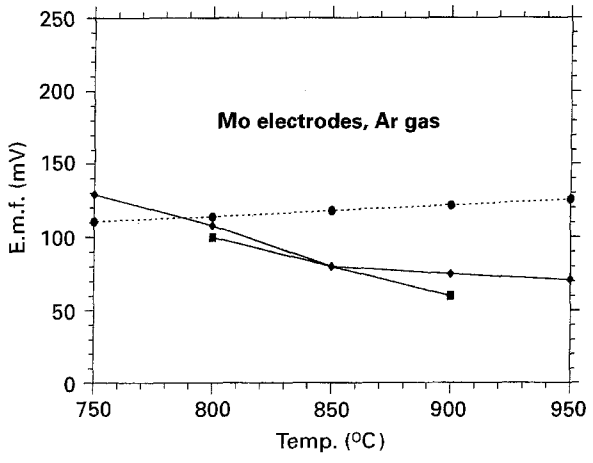

Figure 9 Dwell e.m.f. for the cell $Cr/Cr_2N|Li_3AlN_2|CrN/Cr_2N$. (◆) Experiment 1, (■) experiment 2, (●) Mill's data [15, 16].

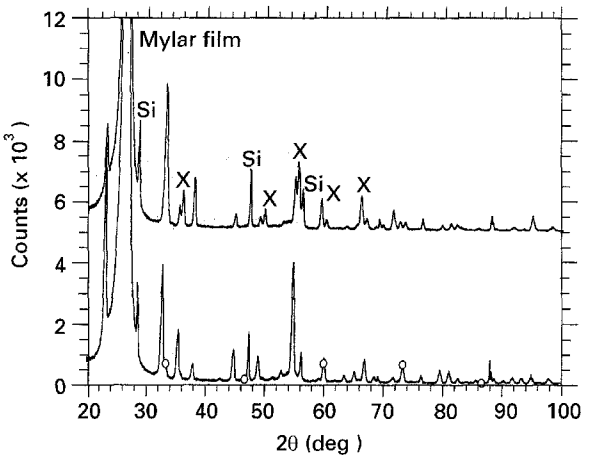

Figure 10 Li_3AlN_2 (O) milled and (—) powdered sintered at 1035 °C. Si = silicon reference, X = aluminium nitride.

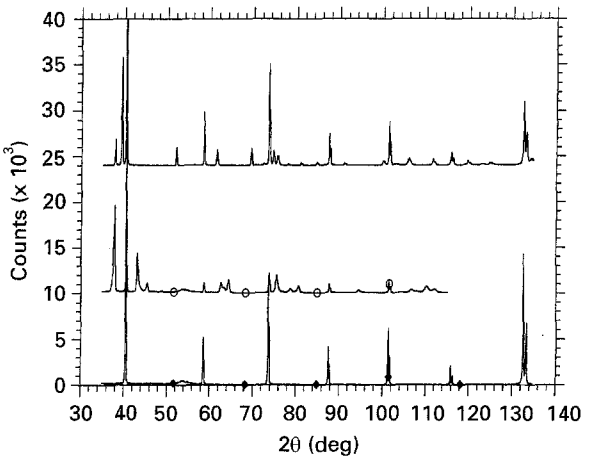

Figure 11 Mo/Mo_2N reference used in thermodynamic measurements with Li_3AlN_2. (◆) molybdenum starting material, (O) Mo_2N starting material, (—) Mo/Mo_2N used in e.m.f. cell.

Cells incorporating the molybdenum reference disagreed markedly with the data of Mills [15, 16] and Wicks and Block [17]. The X-ray diffractogram of Fig. 11 shows that the Mo/Mo_2N reference is unstable and dissociates into another phase. However, as there are no X-ray data available for the other molybdenum nitride phases, namely Mo_3N_2 and Mo_4N_5, it is difficult to identify the unknown phase in Fig. 11 and no thermodynamic data are available.

4. Conclusion

It was found that Li_3AlN_2 and Li_2SiN_2 can be synthesized as a single phase from the solid-state synthesis of Li_3N and AlN for Li_3AlN_2 and Li_3N and β-Si_3N_4 for Li_2SiN_2.

A.c. impedance measurements on Li_3AlN_2 and Li_2SiN_2 gave values of the conductivity which were similar to those found in the literature.

The thermodynamic measurements revealed that Li_3AlN_2 was the best solid electrolyte for producing e.m.f. data close to those of Mills [15, 16] for the Cr/Cr_2N and CrN/Cr_2N references in a temperature range of 750–850 °C. Higher temperature measurements showed a lowering of the e.m.f. which was attributed to a decomposition of Li_3AlN_2 into Li_3N and AlN.

Acknowledgements

The authors are grateful to the SERC and British Steel PIC, for a case award for M.S. Bhamra.

References

1. W. B. MORRISON, *Ironmaking Steelmaking* **16** (2) (1975) 123.
2. R. S. YOUNG, "Chemical Analysis in Extractive Metallurgy" (Charles Criffin, London, 1971) pp. 251–7.
3. T. S. HARRISON, "Handbook of Analytical Control of Iron and Steel Production" (Ellis Horwood, Chichester, 1979) pp. 280–374.
4. D. L. HARRIS, "Quantitative Chemical Analysis" (Freeman, New York, 1987).
5. K. S. GOTO, "Solid State Electrochemistry and its Applications to Sensors and Electronic Devices" (Elsevier, Amsterdam, 1988).
6. A. RABENAU, *Festkorperprobleme* **XVIII** (1978) 77.
7. *Idem, Solid State Ionics* **6** (1982) 277.
8. R. JUZA and F. HUND *Z. Anorg. Allg. Chem.* **257** (1948) 13.
9. H. YAMANE, S. KIKKAWA and M. KOIZUMI, *Solid State Ionics* **15** (1985) 51.
10. R. JUZA, H. H. WEBER and E. MEYER-SHIMON, *Z. Anorg. Allg. Chem.* **273** (1948) 48.
11. J. LANG and J. P. CHARLOT *Rev. Chim. Miner.* **7** (1970) 121.
12. A. T. DADD, and P. HUBBERSTEY, *J. Chem. Soc. Dalt. Trans.* (1982) 2175.
13. J. DAVID, J. P. CHARLOT, and J. LANG *Rev. Chim. Miner.* **2** (1974) 405.
14. H. YAMANE, S. KIKKAWA and M. KOIZUMI, *Solid State Ionics* **25** (1987) 183.
15. T. MILLS, *J. Less Common Metals* **22** (1970) 373.
16. *Idem, ibid.* **26** (1972) 223.
17. C. E. WICKS, and F. E. BLOCK, *Bull. Bur. Mines* **65** (1963) 82.

Received 10 March
and accepted 5 April 1995